CHARM High-Energy Ions for Microelectronics Reliability Assurance (CHIMERA)

Kacper Bilko, *Graduate Student Member, IEEE*, Rubén García Alía, *Member, IEEE*, Alessandra Costantino, Andrea Coronetti, *Associate Member, IEEE*, Salvatore Danzeca, Marc Delrieux, Natalia Emriskova, Matthew Alexander Fraser, Sylvain Girard, *Senior Member, IEEE*, Eliott Philippe Johnson, Marc Sebban, Federico Ravotti, *Member, IEEE*, and Andreas Waets

***Abstract*— We present the progress related to CERN's capacity of delivering highly penetrating, high-linear energy transfer (LET) heavy ions for radiation effect testing of electronic components within the CHARM High-energy Ions for Micro Electronics Reliability Assurance (CHIMERA) project. Profiting from the existing accelerator infrastructure, Monte Carlo simulations, and a 300-μm-thick silicon diode, we highlight the beam characterization capabilities and a summary of the beam properties. Finally, we present the comparison of the static random access memories (SRAMs) single event effect (SEE) cross section measurements with respect to other heavy ion facilities.**

***Index Terms*— Beam characterization, CERN, diode, electronics testing, high energy heavy ions, high linear energy transfer (LET), silicon, single event effect (SEE), single event upset (SEU).**

I. Introduction

VERY High Energy (VHE, >100 MeV/u) heavy ions, typically with $Z \geq 80$ to obtain large enough linear energy transfer (LET) values, are in high demand for radiation effects electronics testing due to their capacity of more directly mimicking the radiation effects induced by galactic cosmic ray (GCR) ion spectra [1], with the highest importance of the 0.1–1 GeV/u energy range [2]. Moreover, due to their high ranges in the matter, their use allows testing in air and removes the need for sample preparation, e.g., delidding or substrate thinning. The last point is particularly important for state-of-the-art, high-performance microelectronic chips. Complex packaging architectures (e.g., flip-chip, stacked chips, 3-D structures, system-in-package) prevent using standard energy ions, typically in 10–20 MeV/u range [3], [4], due to the limited ion penetration. Finally, VHE ions can potentially enable performing tests at a board and even at a box level [5].

Motivated by this need, in 2017, the Radiation to Electronics (R2E) project at CERN initiated efforts aimed at developing VHE ion beams for radiation effects testing within its accelerators and experimental areas infrastructure.

This activity involved using xenon and lead ion beams in the East and North experimental areas at CERN, the first of which is fed by the proton synchrotron (PS) [6], with an ion energy of 5.4 GeV/u, and the second of which is provided beam from the Super PS [7], [8], with an energy range of 13–150 GeV/u. Whereas heavy ion operation in the North Area (NA) is of routine practice for multiple physics experiments at CERN [9], the radiation effects activity was the first in requesting heavy ions to the East Area (EA). Therefore, the successful heavy ion beam extraction during the second half of CERN's Large Hadron Collider (LHC) Run 2 (2017–2018) can be considered an important milestone within the overall activity.

In the NA, several experiments were performed to learn from the heavy-ion beams [10], [11], [12]. Despite the flexibility of NA in terms of ion flux tuning, the energies are too large to provide LETs meaningful for radiation hardness assurance (RHA), even for the heaviest ions in the periodic table.

In the EA, throughout two experimental runs in 2017 and 2018, during which ultrahigh energy (UHE, >5 GeV/u) ions were used to perform radiation effects testing [3], [4], [13], [14], the following limitations were identified. First, only a single beam energy was available, resulting in the LET of $\sim$8 MeV/(mg/cm^2) Second, the machine was configured for very high intensities, not suited for single-event effect (SEE) testing. Finally, the existing beam instrumentation was calibrated for proton operation only.

Despite these limitations and motivated by the worldwide scarcity of VHE ion irradiation facilities and the increasing demand, CERN decided to continue working toward increasing the readiness level for radiation effect testing of its in-house ion irradiation capabilities with technical and financial support from the European Space Agency (ESA). The CHARM High-energy Ions for Micro Electronics Reliability Assurance (CHIMERA) activity was launched in 2020 and implemented

Manuscript received 29 September 2023; revised 24 November 2023 and 27 December 2023; accepted 14 January 2024. Date of publication 25 January 2024; date of current version 16 August 2024. The CHIMERA activity has been supported by the European Space Agency under contracts No. 4000134554 and No. 4000136601. *(Corresponding author: Kacper Bilko.)*

Kacper Bilko is with CERN, 1211 Geneva, Switzerland, and also with CNRS 5516, IOGS, Laboratory Hubert Curien, University of Lyon, Université Jean Monnet, 42000 Saint-Étienne, France (e-mail: kacper.bilko@cern.ch).

Rubén García Alía is with CERN, 1211 Geneva, Switzerland.

Alessandra Costantino is with the European Space Agency, ESTEC, 2201 AZ Noordwijk, The Netherlands.

Andrea Coronetti, Salvatore Danzeca, Marc Delrieux, Natalia Emriskova, Matthew Alexander Fraser, Eliott Philippe Johnson, and Federico Ravotti are with CERN, 1211 Geneva, Switzerland.

Sylvain Girard is with CNRS 5516, IOGS, Laboratory Hubert Curien, University of Lyon, Université Jean Monnet, 42000 Saint-Étienne, France, and also with the Ministére de l'Enseignement Supérieur et de la Recherche, Institut Universitaire de France (IUF), 75005 Paris, France.

Marc Sebban is with CNRS 5516, IOGS, Laboratory Hubert Curien, University of Lyon, Université Jean Monnet, 42000 Saint-Étienne, France.

Andreas Waets is with CERN, 1211 Geneva, Switzerland, and also with the Physik-Institut, University of Zurich, 8006 Zürich, Switzerland.

Color versions of one or more figures in this article are available at https://doi.org/10.1109/TNS.2024.3358376.

Digital Object Identifier 10.1109/TNS.2024.3358376

through a short 2-day run in 2021, a 7-day run in 2022, and a few hours repeatability run in 2023 [15], [16], [17].

This work reports on how the CHIMERA activity has contributed to increasing the C level of the CERN EA infrastructure (described in Section II), allowing to tune flux and energy over ranges that are suitable for electronics testing. We describe how the experimental and simulation methods are employed to determine the flux and energy of the beam at the device-under-test (DUT) location (Section III). Moreover, as a demonstration of electronic testing capabilities, we present a set of single event upset (SEU) cross section measurements (Section IV). Finally, the article will also provide a brief outlook of the activity (Section V), in terms of future steps to further increase the infrastructure readiness level for radiation effects testing, in the context of the European Union (EU)-funded High-Energy Accelerators for Radiation Testing and Shielding (HEARTS) project [18].

II. Facility Layout

A. PS and the East Area

The PS is the third largest CERN accelerator, used both for proton and ion operation. With a circumference of 628 m, it can accelerate protons up to 26 GeV/c and $^{208}Pb^{54+}$ions from 72 MeV/u to ~5.7 GeV/u. In nominal operation, a slow extraction of the beam is implemented to deliver it to the EA, producing spills of 300-400- ms duration. Within the scope of CHIMERA, the most relevant EA facility is CERN High-energy Accelerator Mixed-field (CHARM) [19], where the fully stripped Pb^{82+}ions are delivered through a transfer line of 130 m length. The CHARM facility features a conveyor system that allows precise remote positioning of the DUT. Electrical connection to the DUT is enabled by means of cable chains and a patch panel connecting the irradiation bunker and the control room.

B. Available Beam Instrumentation

The beam intensity in the PS is primarily monitored through a beam current transformer (BCT), measuring a current that is induced in the coils of the device by the presence of a beam. It has been calibrated to provide the number of charges circulating in the accelerator, therefore given the known charge state of $^{208}Pb^{54+}$, the absolute number of ions can be retrieved. The logged BCT measurements are available with 1 ms time resolution.

To provide a beam to the CHIMERA experiments the ions are slowly extracted from the PS over thousands of turns. The beam monitoring is then performed directly along the transfer line, via two types of instruments: secondary emission chambers (SECs) and Ionization Chambers (XIONs), with the latter being significantly more sensitive. The time resolution for both instruments is the same and equal to 20 ms.

The working principle of SECs is as follows: charged particles hit a stack of 5 μm thick stainless steel foils and release a number of secondary electrons which are collected by polarized steel electrodes; this full stack is kept in a vacuum vessel. The amount of collected electrons is proportional to the total number of passing particles. Whereas SEC instruments were calibrated to provide the absolute intensity of proton beams, a dedicated calibration for Pb^{82+}beams is presented in this work.

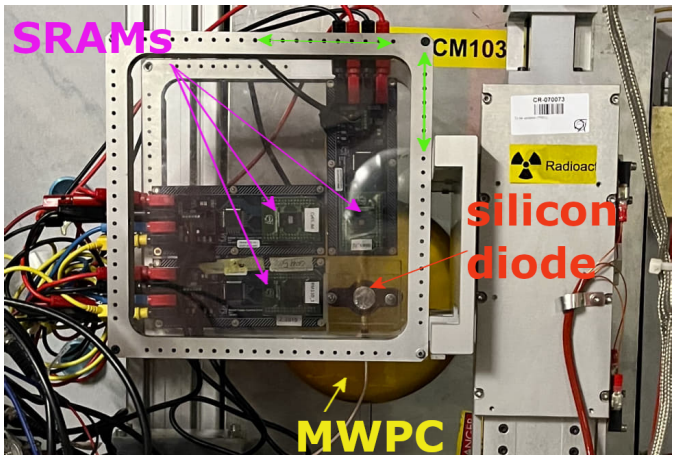

Fig. 1. DUTs employed for the characterization runs of the CHIMERA facility. The DUT frame can be controlled and moved remotely, therefore the DUT (diode or one of the static random access memories) can be swapped without manual intervention.

The XIONs use the same physical principle but for counting primary ion beams. Each XION contains one parallel electrode (5 μm aluminum foils) inside a stainless steel vessel filled with pure Ar gas slightly above atmospheric pressure. The eleven electrodes are connected to a local high-voltage battery supply, whereas the ten charge-collecting foils are connected to the output. The ionization counter works with no avalanche amplification and gives a small but reliable output signal that mirrors the intensity.

The beam at the DUT position is characterized by: 1) a silicon diode detector, for beam flux, time profile, and beam composition; and 2) a multiwire proportional chamber (MWPC) [20], for spatial beam profile. Both instruments are depicted in Fig. 1. The core of the first instrument is a commercial 300- μm–thick silicon diode manufactured by Canberra (model: FD 50-14-300 RM), operated under a reverse bias voltage of 110 V (full depletion). The signal is amplified by a CIVDEC C1-HV and digitized via CAEN DT5751 1 GS/s digitizer. Similar setups are widely used for the heavy-ion beams characterization [21], [22], [23].

The MWPC contains 32 wires both horizontally and vertically. The wire spacing is 6 mm, leading to the coverage of almost 10 $\times$ 10 cm^2 area. The instrument can be operated with different voltages to accommodate both low and high beam intensities.

III. Beam Characterization

A. Beam Energy and Intensity Tuning in the PS

Before entering the PS, the ions are pre-accelerated by means of the Linac3 and the low energy ion ring (LEIR) [24], [25]. The PS operates in cycles, each one containing a single beam injection and ending with the complete beam extraction (or disposal on the dump block). Each cycle delivering beam to EA has a duration of 2.4 s. The technique chosen for beam extraction is the Radio Frequency Knock-Out (RFKO) method. It was selected for its simplicity, as it only requires

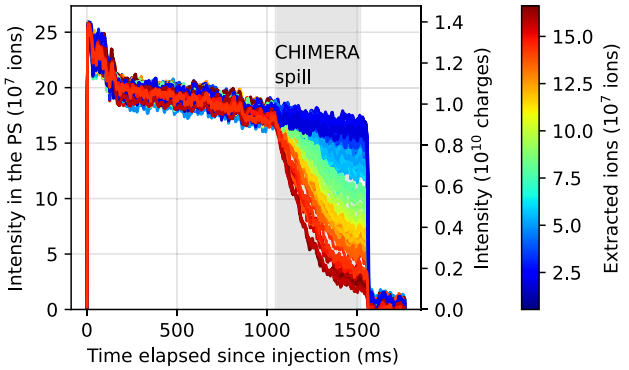

Fig. 2. BCT-measured intensity in the PS accelerator as a function of time during the CHIMERA cycles (energy of the beam 750 MeV/u, 25×10^7 injected lead ions). The period when the beam is slow extracted toward DUT was highlighted. At the end of each cycle, the remaining intensity is sent to a dump (step after 1500 ms). Depending on the requested intensity at DUT, different amount of ions is extracted from the PS accelerator, as illustrated by the varying trace color.

modulating the radio frequency applied to the beam, making it easier to control and maintain. It provides a broad range of extracted beam intensities. The compatibility with existing hardware in the PS also contributed to the choice of the RFKO method [16], [17]. The examples of CHIMERA spills are depicted in Fig. 2. Depending on the RFKO modulation gain, a different number of ions is extracted from the PS toward the EA beamline, thus CHIMERA's DUTs. The ions that were not extracted are sent to a dump at the end of a cycle.

The PS offers a wide range of capabilities, including the potential to extract various ion species (lead, oxygen) and energies, depending on the needs of the experiments. To date, the PS has successfully extracted Pb ions at various energies, such as 1 GeV/u, 750 MeV/u, and 650 MeV/u, demonstrating its versatility and capacity at catering diverse experimental requirements. Once requested, the change between the energies and the intensity tuning is instantaneous.

B. Simulated Beam Energy and LET at Device Under Test

The T08 beamline and associated test facilities in the PS EA were designed to accommodate penetrating 24 GeV/c proton beams. The transport of heavy ions at lower energies (per nucleon) through the transfer line is instead more impacted by the various sections of air (∼30 m), vacuum windows, and beam instrumentation, than that of top energy protons. A dedicated FLUKA [26], [27], [28] Monte Carlo simulation model was constructed in order to: 1) clarify the constraints of experimental beam development activities; 2) deepen the understanding of the beam characteristics at the DUT position as shown by the available instrumentation; and 3) address possible design optimizations in the near future, all aimed at the outcome of commissioning a VHE ion facility for radiation effects testing [29].

The primary quantities of interest that can be extracted from the simulations are the beam transmission, the beam energy, the associated LET at the DUT position, and the beam size. These are all affected by beam-material interactions, most notably electronic stopping (dE/dx) and scattering through Coulomb interactions and inelastic collisions resulting in nuclear fragmentation. A summary of the simulated quantities is given in Table I for a number of representative primary beam

TABLE I

BEAM PARAMETERS AT THE DUT LOCATION AS RETRIEVED THROUGH FLUKA MONTE CARLO SIMULATIONS. THE ION RANGE IN SILICON AT DUT WAS RETRIEVED VIA SRIM [30] ASSUMING THE ENERGY AS GIVEN BY FLUKA

Extracted energy from PS	[MeV/u]	**1000**	**750**	**650**
Transmission PS to DUT	[%]	11.8	4.3	1.3
Energy at DUT	[MeV/u]	605	300	140
LET at DUT	[MeV/(mg/cm^2)]	13.2	18.2	26.6
Range in Si at DUT	[mm]	35	10	3
Gaussian beam size (FWHM)	[cm]	7.48	8.95	9.59

energies extracted from the PS. The simulated beam transmission is defined as the probability of reaching the DUT position in CHARM per primary particle simulated. As expected, the transmission is proportional to the beam energy, calculated at 12% for 1 GeV/u kinetic energy extracted from the PS and decreasing for lower energies. The various material sections that the beam crosses cause beam energy straggling. This effect is more significant for the lowest beam energies: a beam extracted at 650 MeV/u arrives at the DUT position with only 140 MeV/u left. By consequence, the resulting range of beam LETs that can be obtained by varying the beam energy is also larger: LETs from 10 to above 30 MeV/(mg/cm^2) can be reached from primary energy tuning alone. Higher LET can be obtained by further degradation directly applied at the DUT position. The calculated beam profiles are Gaussian and remain roughly equal at the DUT position for each simulated energy with a full width at half maximum (FWHM) on the order of 10 cm, in line with experimental measurements, see Table I.

C. Measured Spatial Beam Profile at Device Under Test

The MWPC, located directly behind the DUT, contains 32 wires in each plane, which collect the charge deposited by the beam. During the experiment, the voltage in the ionization chamber was at 1.8 kV, as opposed to 100 V over the standard proton operation. Effectively, the instrument allows measuring horizontal and vertical 1-D projections of the beam's particle density.

For the three considered beams, listed in Table I the profiles can be approximated with a Gaussian function. Related traces with the Gaussian fits are depicted in Fig. 3, whereas the fits' parameters are presented in Table II.

The MWPC will be critical during the CHIMERA facility upgrade, which will involve the delivery of more spatially uniform beams, accomplished by weaker focusing of the beam by the transfer line quadrupole magnets (increasing FWHM) and collimation close to DUT (to cut-off Gaussian tails).

D. Spill Time Profile

As previously described, CHIMERA beams were extracted and delivered over multiple beam turns (so-called slow extraction) with the expected spill duration between 300 and 400 ms. Fig. 4 depicts the averaged spill profiles (for fluences in between $10^4 - 2 \times 10^4$ ions/cm^2/spill) obtained from the SEC calibration covered in Section III-E. The ∼350 ms spill duration was independent of the beam energy (thanks to the RFKO extraction technique) and its intensity.

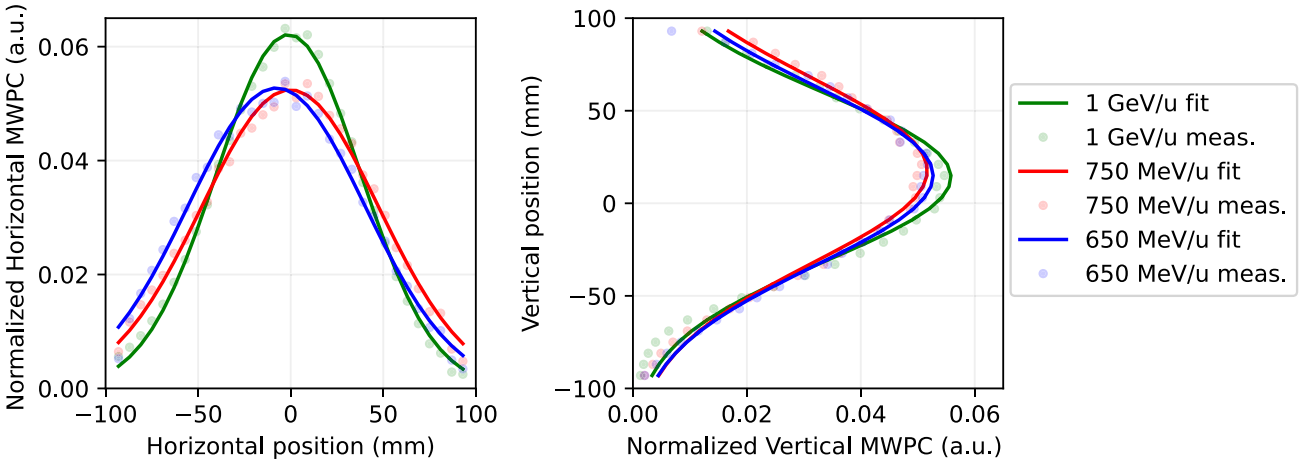

Fig. 3. Gaussian fits for the normalized horizontal and vertical beam profiles at the DUT location as measured by the MWPC for considered ion beams.

TABLE II
PARAMETERS OF THE GAUSSIAN FITS FOR THE SPATIAL PROFILES AS MEASURED BY MWPC INSTRUMENT, WITH THE SIMULATED BEAM FWHM

Beam type	[MeV/u]	1000	750	650
meas. horizontal μ (fit)	[mm]	1.1	-0.3	-7.7
meas. vertical μ (fit)	[mm]	14.1	17.7	14.9
meas. horizontal FWHM (fit)	[cm]	9.2	11.3	11.3
meas. vertical FWHM (fit)	[cm]	10.6	11.8	11.4
simulated FWHM	[cm]	7.5	9.0	9.6

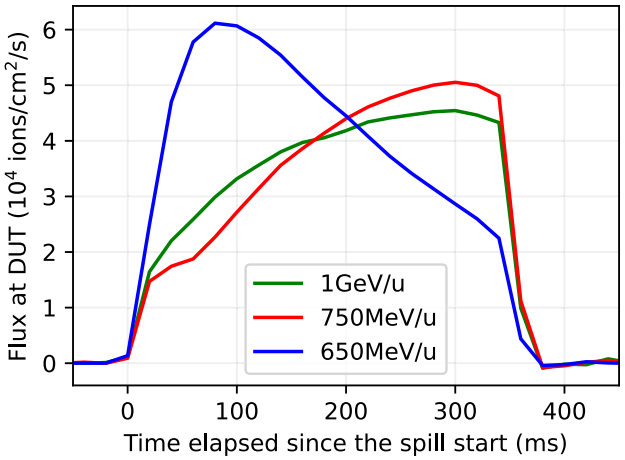

Fig. 4. Averaged flux profile over a spill for three considered beams as measured by the SEC instrument. The selected spills corresponded to fluences between $10^4 - 2 \times 10^4$ ions/cm^2/spill (at the Gaussian maximum).

E. Flux Calibration

For each of the considered beam types (listed in Table I) the calibration of the SEC and XION instruments against the silicon diode detector was performed for the purpose of flux measurements. The silicon detector measures the energy depositions ion by ion, therefore the exact number of ions per spill was retrieved and compared with the counts of the SEC instrument which is in the beam at all times. This allows retrieving the fluence per spill at the center of the beam at the DUT position. Given that both the beam transmission between

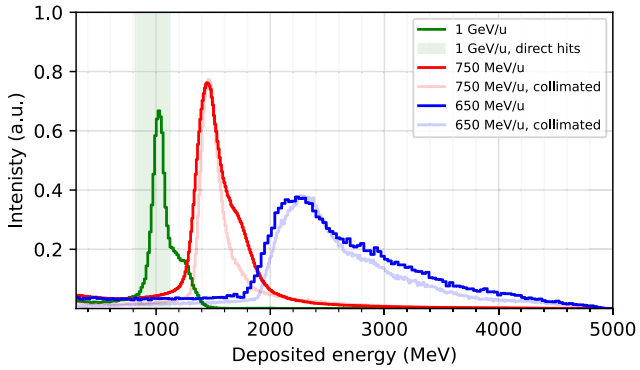

Fig. 5. Spectra of the deposited energies in the silicon diode detector with the highlighted regions corresponding to direct ionization by a main beam. The setup was not optimized for spectroscopy (including the energy resolution) but rather for counting purposes, therefore the large spread in the 650 MeV/u beam does not necessarily reflect the spread in the beam energy or LET. The shaded region for 1 GeV/u beam corresponds to the direct particle hits, i.e., not punching through the detector case. For the 750 and 650 MeV/u beams, complimentary irradiations with the collimator were performed (faded traces). The collimator prevented ions from hitting the detector case.

SEC and DUT position and SEC response might be energy dependent, cross-calibration was independently performed for all three beam types.

There are two main limitations in performing this calibration: 1) the silicon detector has some fraction of the active surface (roughly 40%) under stainless-steel casing, and in the case of 1 GeV/u and 750 MeV/u beams, the energy of the ions is sufficient for punching-through; and 2) for the higher fluxes the buffer of the digitizer saturates, leading to the loss of the single ion resolution. The first limitation was mitigated by performing additional irradiations with a collimator on top of the diode, which allowed the identification of ion beam impact only through the case-uncovered silicon region. Therefore, comparing the shapes of the energy deposition spectra, depicted in Fig. 5 for both normal and collimator cases, enabled to quantify the fraction of events caused by direct hits of a beam onto the exposed silicon surface (0.5 cm^2). The second limitation was mitigated by the optimization of the digitizer settings, focusing on the event rate, and neglecting the analog pulse shapes. The fluence calibration is illustrated

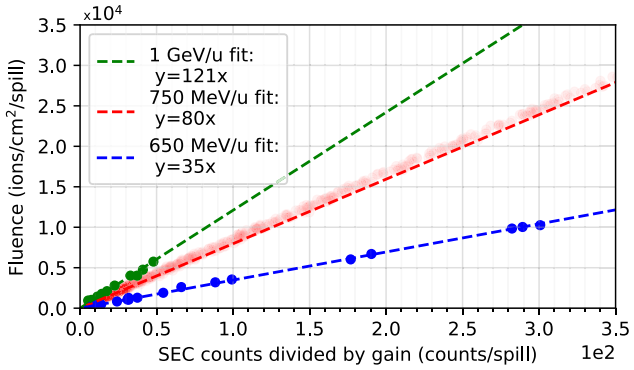

Fig. 6. Fluence per spill measured by silicon diode detector as a function of the SEC counts, with the related linear fits.

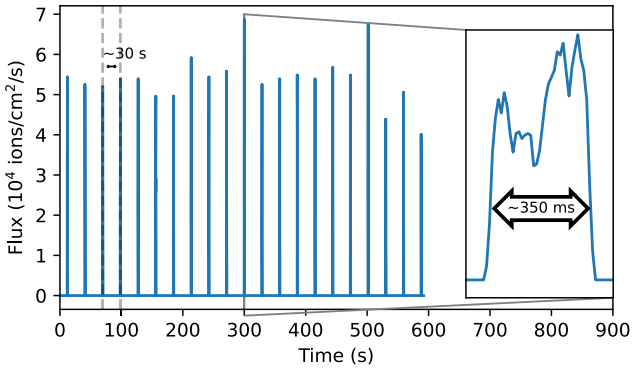

Fig. 7. Beam flux as a function of time as measured by the silicon diode detector. In the presented time period, the 350 ms-long spills are provided to CHIMERA with the 30 s repetition rate, however, the exact timing properties depend on the needs of other PS users. In the most favorable scenario, assuming CHIMERA is the only beam user, each spill would happen every 3.6 s (duration of the cycle in LEIR, the preceding accelerator).

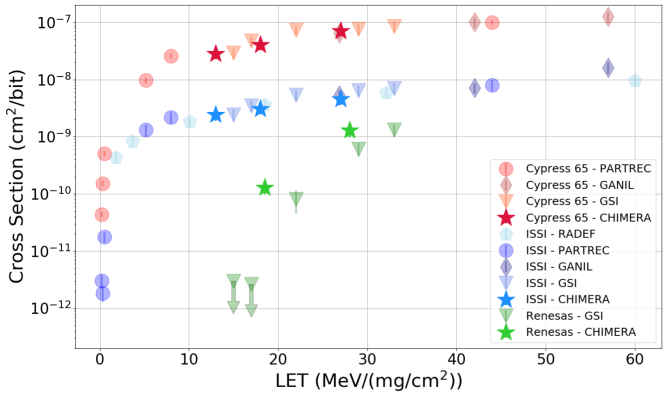

Fig. 8. SEU cross section as a function of ion LET of three SRAMs measured at CHIMERA and compared to other European heavy-ion facilities.

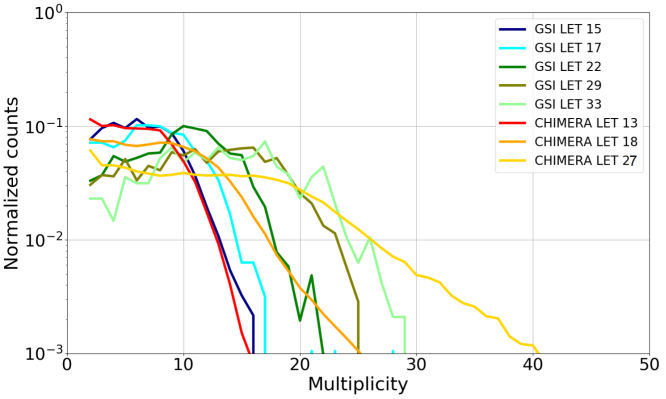

Fig. 9. Histograms of multiplicity distributions measured at GSI compared to those measured at CHIMERA (Cypress SRAM).

in Fig. 6. The calibration factors that needed to be applied to the SEC counts vary depending on the beam energy, suggesting: 1) energy-dependent SEC response and 2) loss of the beam intensity between SEC and DUT (approximately 30 m distance). Given the very strong linearity between both variables, the main source of uncertainty arises from the systematic error in the energy-dependent SEC response and related mitigation procedure. This calibration is critical for the facility users and allows knowing the fluence for each spill, based on the permanently installed instruments, when the diode is replaced with an actual DUT.

Over the experimental irradiations, the delivered fluence per spill spanned between 10^2 and 10^5 ions/cm^2/spill. Typically, every spill, lasting ~350 ms, was delivered every 30 s, as depicted in Fig. 7.

IV. SEE Measurements and Comparison With Other Facilities

Benchmark SEU measurements were performed on three commercial static random access memories (SRAMs): Cypress 65 nm (16 Mbit, part number: CY62167GE30-45ZXI), Integrated Silicon Solution Inc (ISSI) 40 nm (32 Mbit, part number: IS61WV204816BLL-10TLI), Renesas 110 nm (8 Mbit, RMLV0816BGA-4S2). The SRAMs were tested at nominal 3.3 V I/O voltage, with a checkerboard pattern and read after each spill. The Cypress and ISSI SRAMs were irradiated in delidded configuration to reproduce previous irradiation conditions in other facilities. The Renesas SRAM was irradiated lid-on because this was the same configuration for the only other irradiation that happened at GSI. Data were collected in October 2022 and the fluxes and fluences were provided as explained in Section III-E.

Fig. 8 reports the SEU cross sections measured at CHIMERA for the three SRAMs at three different LETs [13, 18, 27 MeV/(mg/cm^2)]. For the Renesas SRAM, measurements at the lowest LET were not done following the previous GSI measurements showing a LET threshold above this value. The SEU cross sections from CHIMERA in the figure are compared with those collected at other European facilities, such as RADEF, PARTREC, GANIL, and GSI [31], [32]. The data in the plots are reported with error bars with a 95% confidence level based on uncertainty on the fluence of 10% for all facilities and on the number of SEUs observed. Error bars dominated by the fluence are typically smaller than the markers and not typically visible for CHIMERA data due to the full opacity of the markers. For the other facilities, they are visible through the marker transparency. Concerning GSI data at the lowest LET for this SRAM, the arrows are meant to indicate that these are upper bounds because no SEUs were measured.

Concerning the comparison of the CHIMERA SEU cross sections with respect to those measured at GSI (similar beam energy) and elsewhere (lower beam energy), the data for the Cypress SRAM provide the best fit to the existing response curve with variations that are within ±20%. The CHIMERA

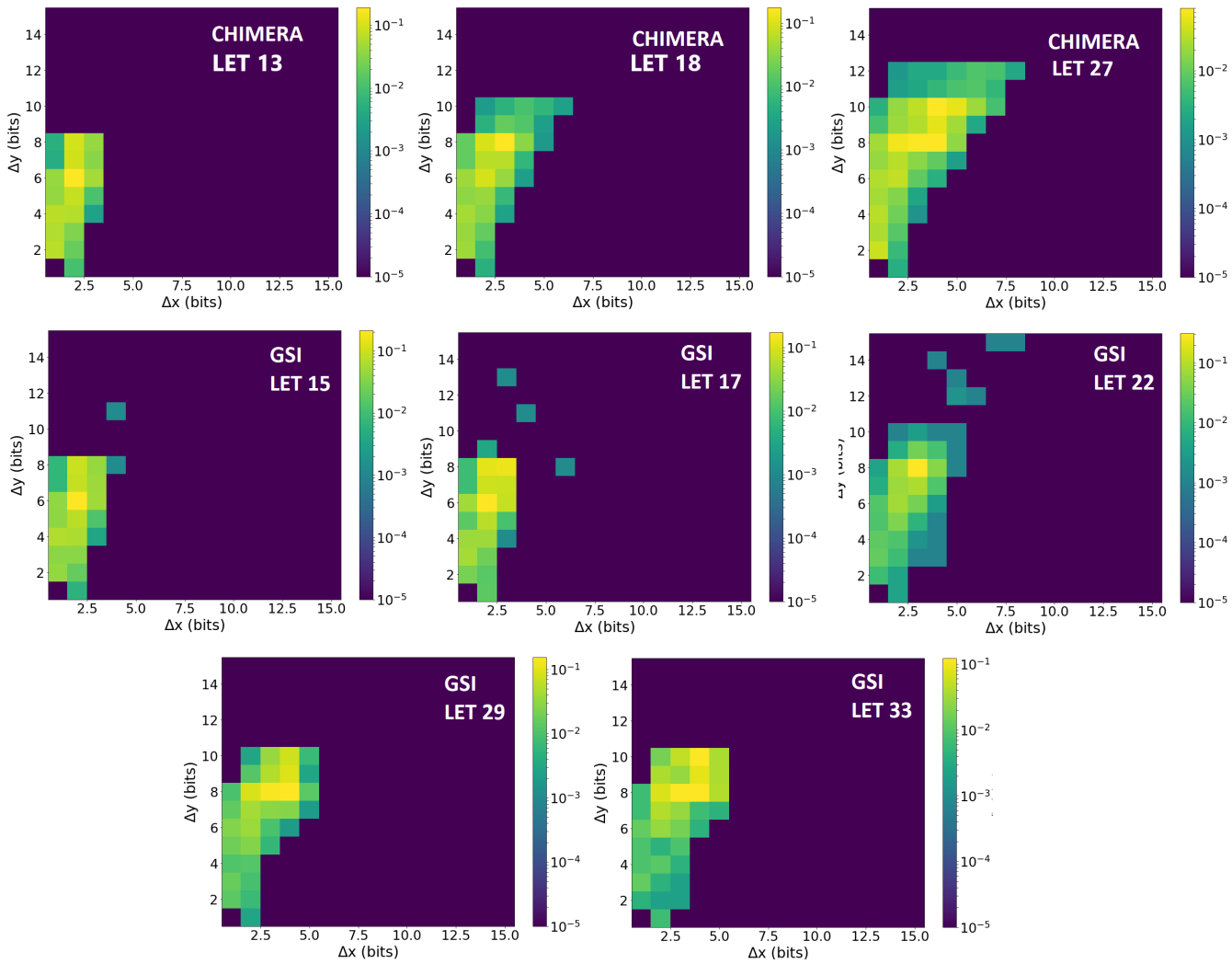

Fig. 10. Heatmaps to characterize MCUs in terms of their bit-wise (horizontal) and word-wise (vertical) extension as a function of the LET of the ion. Data for CHIMERA are compared to GSI. The color scale indicates the probability that an MCU would have a certain horizontal or vertical dimension.

points for the ISSI SRAM all fall slightly above the curve with a maximum discrepancy of a factor of 1.8. Concerning the Renesas, less can be said given that only data at GSI were collected so far. In general, the data collected during 2022 seem to fit in the curve with a maximum discrepancy of a factor of 2.

The Cypress SRAM results can also be analyzed in terms of multiple-cell upsets (MCUs) thanks to a collaboration with LIRMM [33], [34]. This memory is known to suffer from MCUs of very high multiplicity for the ions available in this facility [32]. Differently from other facilities that provide continuous low-flux ion beams, CHIMERA provides 300-ms long spills with rather high intensity. Therefore, time-wise, MCUs can only be separated on a spill-by-spill basis and there is a higher likelihood that two independent MCUs may be mistaken for one. The Manhattan distance used for the MCU classification is 3 bits both in the bit-wise and word-wise directions.

The MCU multiplicity provides a first comparison among the MCU data collected at CHIMERA and those in other facilities. Fig. 9 show MCU multiplicity histograms for several ion beams as a function of their LET. Concerning the ion MCUs measured elsewhere, it is noted that the distributions typically have a plateau that goes from a multiplicity of 2 up to a certain maximum. After that, the probability of having higher multiplicity MCUs falls off very sharply. This is visible in spite of the low statistics for all the runs. Concerning the CHIMERA data, note that this behavior is encountered for the 1 GeV/n case, in which the red curve seems to fall just before the 15 MeV/(mg/cm^2) histogram measured at GSI and also confirming that the LET estimations for CHIMERA at this energy are accurate. For the two higher energies at CHIMERA, however, the histograms do not fall off as sharply after the maximum and they actually display a long tail that extends toward MCU multiplicities that would be more common for higher LET ion beams. The data reported in the figure have already been filtered to remove as much as possible outliers, i.e., removing all MCUs with a likelihood lower than 1 in 1000. This effect is not fully understood. Some possible explanations are: 1) the overlap of MCUs coming from different particles that are merged together and cannot be disentangled with the simple Manhattan

distance approach that worked for lower flux facilities; such kind of effect would have an impact on the MCU analysis while not affecting the SEU cross section determination in which all bit flips are treated singularly and 2) the presence of fragmented ions in the beam that provide a wider LET range.

Other than the multiplicity, MCUs can also be classified by means of a 2-D heatmap representation showing the likelihood that an MCU will have a certain extension in bit-wise (horizontal) or word-wise (vertical) direction. Again, beams with similar LETs would be expected to have similar distributions also in this type of representation. For the sake of conciseness, the comparison is performed between the CHIMERA and the GSI data. The data are reported in Fig. 10. As already demonstrated by the multiplicity, the CHIMERA beam at the lowest LET yields very similar distributions of MCUs as the lowest LET at GSI. The situation at higher LETs for CHIMERA is a bit more complicated. Indeed, if sticking to the maximum likelihoods (yellow in the picture), the MCUs for the CHIMERA 750 MeV/n run tends to be identical to those at GSI for an LET of 17 MeV/(mg/cm^2). However, there is a nonnegligible amount of events surrounding the maximum multiplicity that were either not this numerous or not there at all when testing at GSI. A very similar situation is seen for the CHIMERA 650 MeV/n beam. In fact, at GSI the maximum likelihood is concentrated around MCUs of 8–10 extension in y and 2–4 in x for the 29 MeV/(mg/cm^2) and, why this happens also for CHIMERA, the likelihood around this region is far higher than what was seen at GSI. The same three explanations provided for the differences in the multiplicity distribution apply here.

In conclusion, it can be said that a reasonable agreement was obtained when considering the SEU cross sections measured at CHIMERA with respect to those measured elsewhere no matter if at the same or lower energy. Nevertheless, the MCU analysis leaves some open questions for the two highest LET beams that were employed at CHIMERA and their differences with respect to GSI beams and the other facilities that will require further investigation.

V. Conclusion and Outlook

This article presents the status of the CHIMERA activity, which profits from the existing CERN infrastructure (available accelerators and the CHARM facility), and aims at delivering VHE ion beams with both the high LET and large Si-range. In the longer term, the activity will allow: 1) to control and understand high-energy heavy-ion beams and how they interact with matter and, more specifically, electronics; 2) to develop best practices and guidelines for high-energy heavy ion radiation effects testing; and 3) to reach a readiness level sufficient to render the facility accessible to and exploitable by external users.

Within this work, we presented the available beams (as of 2023) along with their main characteristics: three LET values (13, 18 and 27 MeV/(mg/cm^2), variable intensity in the 10^2 and 10^5 ions/cm^2/spill, Gaussian beam with FWHM of $\sim$10 cm in both horizontal and vertical axes. The presented satisfactory agreement of SRAMs cross section measurements with other facilities indirectly proves the correctness of the dosimetry approach that takes into account: 1) measured intensity values, obtained via SEC instrument, and calibrated by the silicon diode detector; and 2) the simulated LET values at the DUT location.

In November 2022, following various internal beam studies, a beam was for the first time successfully delivered to an external user team from ESA. Furthermore, through the commercial silicon diode detector, the existing beam instrumentation was calibrated to provide accurate online flux measurements. It was demonstrated that the fluence per spill could be varied within three orders of magnitude.

Aiming at delivering spatially uniform beams with a variable LET reaching 40 MeV/(mg/cm^2) with improved beam characterization and dosimetry, accessible to the users via user-friendly access workflow, the continuation of the CHIMERA activity is possible thanks to the HEARTS project funded by the European Commission.

Acknowledgment

The authors would like to acknowledge Luigi Dilillo and the LIRMM team at the University of Montpellier, France, for having performed the data analysis required to determine the MCUs from the raw data in our SRAMs. They also acknowledge Helmut Puchner from Infineon, San Jose, CA, USA, for having provided the information required to disable the ECC of the Cypress 65-nm SRAM.

References

[1] R. G. Alía et al., "Fragmented high-energy heavy-ion beams for electronics testing," *IEEE Trans. Nucl. Sci.*, vol. 70, no. 4, pp. 486–495, Apr. 2023.

[2] R. A. Mewaldt, "Galactic cosmic ray composition and energy spectra," *Adv. Space Res.*, vol. 14, no. 10, pp. 737–747, Oct. 1994. [Online]. Available: https://www.sciencedirect.com/science/article/pii/0273117794905363

[3] M. Kastriotou et al., "Single event effect testing with ultrahigh energy heavy ion beams," *IEEE Trans. Nucl. Sci.*, vol. 67, no. 1, pp. 63–70, Jan. 2020.

[4] R. G. Alía et al., "Ultraenergetic heavy-ion beams in the CERN accelerator complex for radiation effects testing," *IEEE Trans. Nucl. Sci.*, vol. 66, no. 1, pp. 458–465, Jan. 2019.

[5] A. de Bibikoff and P. Lamberbourg, "Method for system-level testing of COTS electronic board under high-energy heavy ions," *IEEE Trans. Nucl. Sci.*, vol. 67, no. 10, pp. 2179–2187, Oct. 2020.

[6] J. Bernhard, F. Carvalho, S. Evrard, E. Harrouch, and G. Romagnoli. (Dec. 2021). *CERN Yellow Reports: Monographs, Vol. 4 (2021): CERN Proton Synchrotron East Area Facility: Upgrades and Renovation During Long Shutdown 2*. [Online]. Available: https://e-publishing.cern.ch/index.php/CYRM/issue/view/145

[7] P. Collier and B. Goddard, "The SPS as LHC injector," in *Proc. Part. Accel. Conf.*, vol. 4, Jun. 2001, pp. 3150–3152.

[8] K. Bilko et al., "CERN super proton synchrotron radiation environment and related radiation hardness assurance implications," *IEEE Trans. Nucl. Sci.*, vol. 70, no. 8, pp. 1606–1615, Aug. 2023.

[9] D. Banerjee. (Jul. 2021). *The North Experimental Area at the CERN Super Proton Synchrotron*. [Online]. Available: https://cds.cern.ch/record/2774716

[10] V. Wyrwoll et al., "Heavy ion nuclear reaction impact on SEE testing: From standard to ultra-high energies," *IEEE Trans. Nucl. Sci.*, vol. 67, no. 7, pp. 1590–1598, Jul. 2020.

[11] V. Wyrwoll et al., "Longitudinal direct ionization impact of heavy ions on see testing for ultrahigh energies," *IEEE Trans. Nucl. Sci.*, vol. 67, no. 7, pp. 1530–1539, Jul. 2020.

[12] M. Glorieux et al., "Single-event characterization of Xilinx UltraScale+® MPSOC under standard and ultra-high energy heavy-ion irradiation," in *Proc. IEEE Nucl. Space Radiat. Effects Conf. (NSREC)*, Jul. 2018, pp. 189–193.

[13] P. F. Martinez et al., "SEE tests with ultra energetic Xe ion beam in the CHARM facility at CERN," *IEEE Trans. Nucl. Sci.*, vol. 66, no. 7, pp. 1523–1531, Jul. 2019.

[14] T. Rajkowski et al., "Analysis of SET propagation in a system in package point of load converter," *IEEE Trans. Nucl. Sci.*, vol. 67, no. 7, pp. 1494–1502, Jul. 2020.

[15] M. Fraser et al., "Feasibility of slow-extracted high-energy ions from the CERN proton synchrotron for CHARM," in *Proc. 13th Int. Particle Accelerator Conf. (IPAC)*, Geneva, Switzerland: JACOW Publishing, Jun. 2022, pp. 1703–1706. [Online]. Available: https://accelconf.web.cern.ch/ipac2022/doi/JACoW-IPAC2022-WEPOST012.html

[16] M. Delrieux et al., "Production of slow extracted beams for CERN's east area at the proton synchrotron," in *Proc. 14th Int. Part. Accel. Conf.* Geneva, Switzerland: JACoW Publishing, May 2023, pp. 257–260. [Online]. Available: https://indico.jacow.org/event/41/contributions/1036

[17] E. Johnson et al., "Beam delivery of high-energy ion beams for irradiation experiments at the CERN proton synchrotron," in *Proc. 14th Int. Part. Accel. Conf.* Geneva, Switzerland: JACoW Publishing, May 2023, pp. 297–300. [Online]. Available: https://indico.jacow.org/event/41/contributions/1235

[18] CERN. (2023). *HEARTS Project*. Accessed: Sep. 30, 2023. [Online]. Available: https://hearts-project.eu/

[19] J. Mekki et al., "CHARM: A mixed field facility at CERN for radiation tests in ground, atmospheric, space and accelerator representative environments," *IEEE Trans. Nucl. Sci.*, vol. 63, no. 4, pp. 2106–2114, Aug. 2016.

[20] G. Charpak and F. Sauli, "Multiwire proportional chambers and drift chambers," *Nucl. Instrum. Methods*, vol. 162, nos. 1–3, pp. 405–428, Jun. 1979. [Online]. Available: https://www.sciencedirect.com/science/article/pii/0029554X79907262

[21] M. Bagatin et al., "Characterizing high-energy ion beams with PIPS detectors," *IEEE Trans. Nucl. Sci.*, vol. 67, no. 7, pp. 1421–1427, Jul. 2020.

[22] C. Cazzaniga et al., "Measurements of ultra-high energy lead ions using silicon and diamond detectors," *Nucl. Instrum. Methods Phys. Res. A, Accel. Spectrom. Detect. Assoc. Equip.*, vol. 985, Jan. 2021, Art. no. 164671. [Online]. Available: https://linkinghub.elsevier.com/retrieve/pii/S0168900220310688

[23] T. Borel et al., "PIPS diode test setup for heavy ion beam spectral characterization," *IEEE Trans. Nucl. Sci.*, vol. 70, no. 8, pp. 1732–1739, Aug. 2023. [Online]. Available: https://ieeexplore.ieee.org/document/10146309/

[24] N. Biancacci et al., "Linac3, LEIR and PS performance with ions in 2021 and prospects for 2022," in *Proc. 13th Int. Part. Accel. Conf. (IPAC)*, 2021, pp. 1983–1986.

[25] M. Chanel, "LEIR: The low energy ion ring at CERN," *Nucl. Instrum. Methods Phys. Res. A, Accel. Spectrom. Detect. Assoc. Equip.*, vol. 532, nos. 1–2, pp. 137–143, Oct. 2004. [Online]. Available: https://www.sciencedirect.com/science/article/pii/S0168900204011994

[26] C. Ahdida et al., "New capabilities of the FLUKA multi-purpose code," *Frontiers Phys.*, vol. 9, Jan. 2022, Art. no. 788253. [Online]. Available: https://www.frontiersin.org/articles/10.3389/fphy.2021.788253/full

[27] T. T. Böhlen et al., "The FLUKA code: Developments and challenges for high energy and medical applications," *Nucl. Data Sheets*, vol. 120, pp. 211–214, Jun. 2014.

[28] A. Ferrari, P. Sala, A. Fasso, and J. Ranft, "FLUKA: A multi-particle transport code," SLAC Nat. Accel. Lab., Menlo Park, CA, USA, Tech. Rep. SLAC-R-773, Dec. 2005, doi: 10.2172/877507.

[29] A. Waets et al., "Heavy ion beam characterization for radiation effects testing at CERN using Monte Carlo simulations and experimental benchmarking," in *Proc. 14th Int. Part. Accel. Conf.* Geneva, Switzerland: JACoW Publishing, May 2023, pp. 5106–5109. [Online]. Available: https://indico.jacow.org/event/41/contributions/2806

[30] J. F. Ziegler, M. D. Ziegler, and J. P. Biersack, "SRIM—The stopping and range of ions in matter (2010)," *Nucl. Instrum. Methods Phys. Res. Sect. B, Beam Interact. Mater. At.*, vol. 268, nos. 11–12, pp. 1818–1823, Jun. 2010. [Online]. Available: https://ui.adsabs.harvard.edu/abs/2010NIMPB.268.1818Z

[31] A. Coronetti et al., "SEU characterization of commercial and custom-designed SRAMs based on 90 nm technology and below," in *Proc. IEEE Radiat. Effects Data Workshop*, Nov. 2020, pp. 56–63.

[32] R. G. Alía et al., "Heavy ion energy deposition and SEE intercomparison within the RADNEXT irradiation facility network," *IEEE Trans. Nucl. Sci.*, vol. 70, no. 8, pp. 1596–1605, Aug. 2023.

[33] G. Tsiligiannis et al., "Multiple cell upset classification in commercial SRAMs," *IEEE Trans. Nucl. Sci.*, vol. 61, no. 4, pp. 1747–1754, Aug. 2014.

[34] A. Bosser et al., "Investigation on MCU clustering methodologies for cross-section estimation of RAMs," *IEEE Trans. Nucl. Sci.*, vol. 62, no. 6, pp. 2620–2626, Dec. 2015.